Computers and Structures 190 (2017) 162–172

Contents lists available at ScienceDirect

Computers and Structures

journal homepage: www.elsevier.com/locate/compstruc

Artificial Neural Network (ANN) based microstructural prediction model for 22MnB5 boron steel during tailored hot stamping

Prasun Chokshi [a,*], Richard Dashwood [b], Darren J. Hughes [a]

[a] WMG, University of Warwick, Coventry CV4 7AL, UK
[b] Vice-Chancellor's Office, Coventry University, Coventry CV1 5FB, UK

ARTICLE INFO

Article history:
Received 31 March 2017
Accepted 29 May 2017
Available online 15 June 2017

Keywords:
Artificial Neural Network
Tailored hot stamping
Microstructure
Nanoindentation
22MnB5 boron steel
Modelling

ABSTRACT

Because of demand for lower emissions and better crashworthiness, the use of hot stamped 22MnB5 boron steel has greatly increased in manufacturing of automobile components. However, for many applications it is required that only certain regions in hot stamped parts are fully hardened whereas other regions need be more ductile. The innovative process of tailored hot stamping does this by controlling the localized microstructures through tailored cooling rates by dividing the tooling into heated and cooled zones. A barrier to optimal application of this technique is the lack of reliable phase distribution prediction model for the process.

We present a novel Artificial Neural Network (ANN) based phase distribution prediction model for tailored hot stamping. The model was developed and validated using data generated from extensive thermo-mechanical physical simulation experiments and instrumented nanoindentation based phase quantification method. Advanced statistical techniques were used for preventing overfitting, for making the optimal use of available experimental data and for quantification of prediction uncertainty. The final predictions made by the ANN model during its independent validation have shown good agreement with the experimentally generated data and have a RMS prediction error of just 7.7%, which is a significant improvement over the existing models.

1. Introduction

Hot stamping is an innovative, non-isothermal forming process in which both forming and quenching occur simultaneously [1]. The microalloyed 22MnB5 boron steel is the most widely used material in the automotive industry for manufacturing of hot stamped parts [2,3]. In recent years there has been a huge increase in the use of hot stamping in the automotive industry. The use of hot stamping offers several advantages including lower forming stresses, minimal springback, greater forming accuracy and high strengths. Also using automobile parts with high strength to weight ratios as produced by hot stamping, helps in meeting the automotive industry's dual requirement of reduced emissions and increased passenger safety [1–4].

The final microstructure produced in the boron steel after the conventional hot stamping consists mainly of martensite along with small amount of other phases. This high martensitic content in the final microstructure of the boron steel leads the formed parts to achieve tensile strengths well in excess of 1500 MPa [1–5]. On the other hand, the high tensile strength of the fully hot stamped parts leads to them having low ductility and poor energy absorption characteristics. Such hot stamped parts therefore are not fully optimized for crash performance and light weighting [6–8]. Researchers have come up with an innovative solution to this problem where local sheet metal cooling rates are varied by dividing the tooling into heated and cooled zones. Doing so introduces local regions within hot stamped parts which have a softer and more ductile microstructure as compared to the rest of the part [9–11]. This process is known as tailored hot stamping and it allows for tailoring of the local mechanical properties in the different regions of the hot stamped parts to fully optimize the energy absorption characteristic of the formed part for improved crash performance and light weighting.

Most of the available scientific literature is focused on experimental investigations of the tailored hot stamping process. However a robust and reliable phase distribution model for tailored hot stamping process is required for the design and production of fully optimized automotive structural and safety components through computer aided engineering (CAE). The final phase distribution which results in the different regions of a tailor hot stamped part is dependent on both the thermal and mechanical history of

* Corresponding author.
E-mail address: P.H.Chokshi@warwick.ac.uk (P. Chokshi).

http://dx.doi.org/10.1016/j.compstruc.2017.05.015
0045-7949/

that region. Several papers in the literature have investigated and reported the significant effect of the deformation on the final phase distribution during hot stamping [12–15]. The majority of early numerical models that have been developed for final phase distribution prediction during hot stamping have had limited success because of their inability to account for the effect of deformation [9,16–19]. The predicted phase volume fractions by such models for a hot stamped part have been off by 30–40% in the regions with deformation. In 2014, Tang et al. [20] developed a fully coupled thermo-mechanical-metallurgical numerical model for tailored hot stamping process using the commercial FE code FORGE™ which attempted to take into account the effect of deformation on phase transformation kinetics for making the final phase distribution prediction. This model performed better than the existing models in some conditions but its performance deteriorated for high deformation regions under high temperature heated tooling. For the highly deformed region in the side wall of a U-channel part formed under a heated die at 723 K, the model ended up predicting a bainite content of 63% whereas the authors suggested that negligible bainite was observed in the microstructure from the region using metallography and microscopy.

Also, all the phase distribution prediction models that have been developed so far for tailored hot stamping process have used metallography and microhardness measurements for phase quantification during model development and validation [9,16–20]. The final microstructure produced in boron steel after tailored hot stamping is a complex mixture of martensite, bainite and ferrite phases depending on the thermal and mechanical processing conditions [1,6–9,20]. Metallography and microhardness measurements are well suited for a qualitative assessment of such complex microstructures generated during tailored hot stamping but these techniques are not suitable for quantification of different phases present in the final microstructure. The phase quantification data generated using these techniques for such complex microstructures will be uncertain and subjective, which places a limitation on the reliability and performance capabilities of the existing models developed using such data.

2. Research approach and theory

In addition to the standard physical models for phase distribution predictions in steels, another approach based on Artificial Neural Networks (ANN) has also been explored in the last decade in the field of steel processing [21–24]. Promising results have been obtained from the models developed using ANN not only for phase distribution prediction but also for other classes of problems in the field of materials processing and manufacturing [25–28]. This approach is particularly suitable for developing models for prediction in cases where the qualitative effects of all the relevant input parameters on the output are known but those effects have not yet been completely quantified by the existing physical models. The knowledge of qualitative effects of input parameters on output is an empirically observed proof of the existence of a functional relationship and ANN based models can be used to learn that functional relationship from experimental data. Once the ANN based model has successfully learnt those functional relationships from experimental data during its training and development, then the ANN based model can be used for guiding engineering decisions.

The power of ANN based modelling lies in its capability to learn any kind of functional relationship present in the experimental data within an arbitrary degree of accuracy and not be limited to a particular class or set of functional relationships. The basic mathematical principle behind an ANN model corresponds to learning from experience (past observations, data) and using the knowledge gained from that to make future predictions. However at the same time because of the powerful flexibility of the ANN model to learn any kind of functional relationship from the data, proper consideration needs to be given to prevent overfitting of the ANN model during its training and development. Also for the neural network model to be reliable, there needs to be a proper quantification of the uncertainties in the predictions made by the model [21,25,29,30].

In this research a novel Artificial Neural Network (ANN) based phase distribution prediction model has been developed for tailor hot stamped 22MnB5 boron steel, which is able to successfully take into account both the thermal and mechanical history while making final phase distribution predictions. In order to develop this ANN based model, extensive thermo-mechanical experiments were performed to physically simulate the thermal and mechanical conditions which the different regions of a tailor hot stamped component undergo during their processing [15,20,31–33]. The phase distributions in the final microstructures of different thermo-mechanical test samples were quantified using cutting edge scanned surface instrumented nanoindentation technique [34–37].

Using scanned surface instrumented nanoindentation technique allowed for reliable, repeatable and objective quantification of the different phases present in the sample microstructures. The measurements done by nanoindentation were further backed by qualitative assessment of the microstructural images obtained from metallography and optical microscopy. Thus these two techniques used in conjunction provided good quality and robust phase quantification data which was used for the development of the final ANN model. Using such data for the ANN model development ensured that the model learnt from reliable and objective data during its training and development, which is a necessary prerequisite for empirical modelling.

During the development of the ANN model, the limited availability of the experimental data had posed a challenge and so advanced statistical techniques were used for optimal utilization of the data [42–47]. This statistical approach for ANN model development, when faced with the constraint of limited available data, helped in developing an ANN model which was robust to the issue of overfitting. Along with that the statistical approach also helped in exploring the different neural network topologies and harnessing the distinctive advantages of different topologies for the final ANN based model. Finally this approach for model development helped in capturing the localized variations in the prediction confidence of the final ANN model in different regions of the experimental space, which allowed for generation of customized uncertainty bars for each prediction made by the final ANN model.

After that once the final ANN based model had been developed, its prediction performance was rigorously measured and analyzed. The ANN model was validated by measuring its performance over completely new and independent data from additional thermo-mechanical physical simulation experiments.

3. Experimental work for physical simulation of tailored hot stamping

The material used for the experiments was HQ1500 CR boron steel (22MnB5) sheet with a thickness of 1.5 mm. It is a commercial grade uncoated boron steel sheet developed by Tata Steel specifically for hot forming. The chemical composition of steel is presented in Table 1.

A total of 50 Gleeble tests were performed using dog bone shaped coupons that physically simulated at laboratory scale the various thermal and mechanical conditions which occur in different regions of a formed part during industrial tailored hot stamping. During the Gleeble tests, all the samples were heated up to

Table 1
Average chemical composition of steel used in experimental work in wt%.

C	Mn	Cr	Si	Ti	N	B	Ca
0.22	1.228	0.288	0.165	0.023	0.0051	0.0032	0.0016

temperatures above 1173 K from room temperature at an average heating rate of 10 K/s. The samples were kept above 1173 K for a minimum of 5 min to simulate furnace heating during tailored hot stamping. This ensured that all the Gleeble test samples had a fully austenitic microstructure without any significant grain coarsening before the cooling simulation commenced [33].

For each sample initially after austenitization, until the deformation temperature was reached, the thermal paths simulated the air cooling which occurs while a blank is being transferred from furnace to press. Then at different preset temperatures of deformation (ranging from 1133 K to 973 K), different samples underwent varying amount of isothermal tensile deformations. These tensile deformations simulated the different strain amounts which occur in different regions of tailor hot stamped parts during forming. All the tensile deformations were performed at a fixed strain rate value of 1 s^{-1}. After the deformation all the samples continued on their individual thermal paths. The different thermal paths to be followed by the Gleeble samples after deformation were designed using the thermal history data for tailored hot stamping available from literature and simulated die temperatures ranging from room temperature to 823 K [9,20,38]. The main objective behind designing these thermal paths was to physically simulate the tailored hot stamping thermal conditions as closely as possible during Gleeble testing based thermos-mechanical simulation of the process. A detailed description of the Gleeble based thermo-mechanical experiments done for physical simulation of the tailored hot stamping process is present in the PhD thesis of Chokshi [41].

Following the Gleeble testing, each sample was cut at the point of the thermo-couple welding using a Buehler IsoMet 4000 linear precision saw. The cross-sectional area of the sample was utilized for phase quantification, as that was the location from where thermal history data had been collected by the thermocouple. All the samples were mounted in thermosetting resin using a Buehler SimpliMet hot mounting press, ground using abrasive paper and then finally polished to a mirror finish using a final stage 0.05 μm diamond suspension polishing medium. The final microstructure produced in the Gleeble samples was a complex mixture of martensite, bainite and ferrite phases. It is common knowledge that each of the microstructural phases in steels has got different hardness and this difference in the hardness levels of individual phases was used to characterize and quantify their relative distribution in the final microstructure with a high degree of reliability and repeatability using scanned surface instrumented nanoindentation technique [34,37,39].

An 18×18 array of nanoindents was taken on the cross-sectional area of each Gleeble test sample with a spacing of 150 μm in x-direction and spacing of 30 μm in y-direction as shown in Fig. 1. The peak load used for nanoindentation testing was fixed at 0.8 g and the dwell period at peak load was 20 s [34,37]. The spacing between the indents was chosen so that it allowed for covering a majority of the cross-sectional surface area while at the same time ensuring that there was significant distance between neighbouring indents. The dimensions of individual nanoindents were of the order of few microns as shown in Fig. 1 and ensured that on average a single nanoindent measured the hardness of a single phase. After the instrumented nanoindentation tests were finished for all the 50 samples, secondary testing was done for a selection of 8 randomly chosen samples for quantifying the uncertainty in phase fraction measurements obtained by nanoindentation. For all these 8 samples, a secondary test with 15×15 nanoindentation array with a spacing of 100 μm in x-direction and a spacing of 30 μm in y-direction was performed with all the remaining parameters staying the same.

For metallographic analysis, all the samples were etched using standard 2% Nital solution. The etched samples were observed under optical microscope at 50× magnification and for each sample three microstructural images at different locations along the cross-sectional surface were recorded. These microstructural images were used for secondary qualitative assessment of the different phases present in the final microstructure.

4. Experimental data and development of the ANN dataset

The input parameters for the ANN model consisted of thermal history of the Gleeble samples, temperature of deformation and the amount of deformation that the sample underwent during Gleeble testing. The thermal history of the samples was recorded using thermocouples welded at the centre of all the samples. All the phase transformations of interest in the sample begin once the cooling starts from the austenitization temperature of 1173 K. Thus the time at 1173 K, after which the cooling process starts, was assigned to be the start point ($t = 0s$) and all the following temperature history data was parameterized by converting it

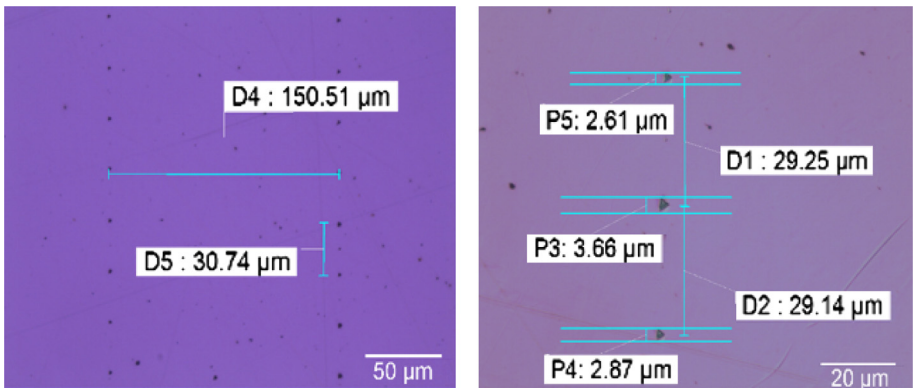

Fig. 1. An array of nanoindents on the surface of a Gleeble test sample.

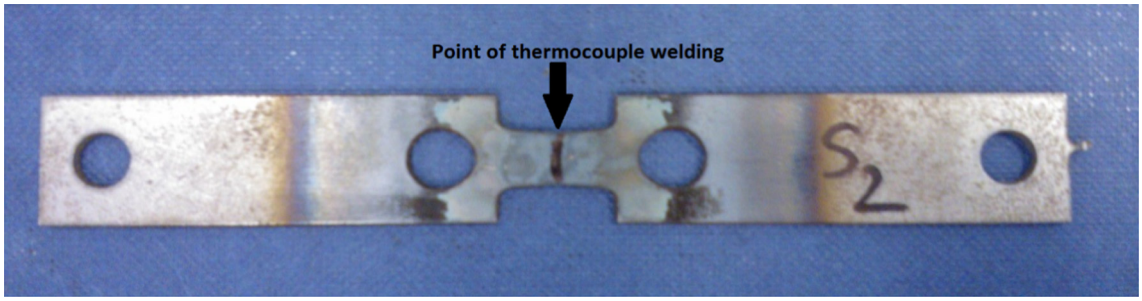

Fig. 2. Gleeble sample with non-uniform elongation after high temperature deformation.

into the following input features: time to 1073 K (s), time to 973 K (s), time to 873 K (s), time to 773 K (s), time to 673 K (s), time to 573 K(s), time to 473 K (s) and time to 373 K (s).

The high temperature tensile deformation during Gleeble tests led to non-uniform elongation in the central region of the sample as shown in Fig. 2 because of the temperature gradient caused by electrical resistance heating. For each tensile deformed sample, the width and thickness at the location of thermocouple welding was measured manually and engineering strain at that location was calculated by applying the principle of volume constancy using the original known volume of the undeformed sample. To reflect the uncertainty in the amount of deformation present, each sample was classified into a strain range class of 5% based on these strain measurement calculations for parametrization of deformation amount. Thus for each sample the amount of deformation present was classified into engineering strain classes such as 0–5%, 5–10%, 10–15%, 15–20%, 20–25% and so on.

The output part of the dataset consists of the different martensite, bainite and ferrite phase volume fractions present in each sample. For each Gleeble test sample, the cross-sectional area was scanned using an 18×18 grid of nanoindents and the hardness data obtained from the nanoindentation test was analyzed to get the phase distribution measurements of the sample. Hardness values less than 200HV were classified as corresponding to ferrite, those between 200 and 400HV were classified as corresponding to bainite and those above 400HV as corresponding to martensite [35–37]. The relative proportion of hardness values for each class, gives us the relative phase distribution of martensite, bainite and ferrite in the final microstructure. In order to measure the uncertainty in the phase distribution quantification obtained from nanoindentation testing, a secondary set of nanoindentation tests were done on a selection of 8 randomly chosen samples. The phase distribution values obtained from these secondary tests were compared with the original values to get an estimate of the variation observed in the phase fraction measurements obtained by nanoindentation testing.

The absolute difference between the phase fraction values obtained from the primary and secondary tests were calculated for all the 8 samples on which secondary testing was done. The average value of absolute difference in the phase volume fraction measurements between the original tests and the secondary tests was found to be 4.7%. The standard deviation for the absolute difference measurements was found to have a value of 3.5%. Thus 3.5% was used as the value of standard deviation and using that an upper limit on uncertainty of 11.7% was calculated, as approximately 95% of observations always fall within 2 standard deviations from the mean ($4.7\% + 2 \times 3.5\% = 11.7\%$). Thus the absolute uncertainty in a phase fraction measurements obtained by instrumented nanoindentation testing was calculated to be 11.7%.

Once all the data had been collected and analyzed it was used to create the final ANN dataset with 50 datapoints corresponding to the 50 Gleeble tests performed. Based on all the experimental data, a final ANN dataset was created which was used for development and validation of the final ANN model. All the input and output features of the ANN dataset along with their range of values are listed in table given below:

5. ANN model development

In this research, a multi-layered feed-forward Artificial Neural Network (ANN) based phase distribution model has been developed [29]. Network topology with one input layer, two hidden layers and one output layer was selected for the work as it has been shown theoretically that such a neural network can model any complex continuous non-linear multivariate functional relationship with a fixed degree of uncertainty [29,40]. This result applies to neural networks which use sigmoidal units in the hidden layers and linear units in the output layer and hence the activation function for the neurons in the hidden layer was selected to be sigmoidal and for the neurons in the output layer was selected to be linear for the final ANN model [29,40]. The input layer consisted of the 10 input nodes which just take on the values of input variables as defined in Table 2 and the output layer consisted of 3 output nodes corresponding to the each of the three phase fractions (martensite, bainite and ferrite) that the final ANN model was supposed to predict.

Each neuron in the hidden layer and output layer has a corresponding set of weights attached with it. For each neuron, all its inputs from the previous layer are multiplied with the corresponding set of weights attached with that neuron and then the linear summation of those products is taken as the input for the activation function of that neuron. Initially the set of weights for each neuron in hidden layer and output layer is randomly chosen and thus the output values predicted by the model do not match with

Table 2
Input and output features of the final ANN dataset.

Input 1	Input 2	Input 3	Input 4	Input 5	Input 6	Input 7	Input 8	Input 9	Input 10	Output
Time to 1073 K (s)	Time to 973 K(s)	Time to 873 K(s)	Time to 773 K (s)	Time to 673 K (s)	Time to 573 K(s)	Time to 473 K(s)	Time to 373 K(s)	Deformation Amount (strain class)	Deformation Temperature (K)	Martensite, Bainite and Ferrite phase fraction values (%)
Cooling process should finish within 180 s after starting at 1173 K (within the range of industry standard)								0–5% to 55–60%	1133–973 K	0–100

the corresponding output values present in training dataset. The output generated by the model is used to calculate the error in the prediction and then weights are iteratively updated so as to reduce this error. This process of iteratively updating the weights of the individual neurons in the neural network to reduce its prediction error, so that it starts to approximate the complex multivariate functional relationship present between input and output parameters in the training dataset, is what constitutes the process of *learning* during ANN based modelling.

For this research work, a classical backpropagation algorithm was used for learning during the training and development of the model [29]. The authors have done their own implementation of the classical backpropagation algorithm in MATLAB and had used that for the final ANN model development. The main reason behind developing the implementation of the backpropagation algorithm from the scratch was to achieve the flexibility in the model training and development process, which was required for the application of the advanced statistical techniques for the final ANN model development.

5.1. Division of ANN dataset, K-fold cross-validation and no. of neurons

The division of the available ANN dataset consisting of 50 datapoints, corresponding to the 50 Gleeble tests, was performed randomly as shown in Fig. 3. Due to the limited availability of the experimental resources, the input dataset for training and development of the final ANN model was limited to a total of 40 datapoints. When the input dataset is divided into a training dataset and a cross validation dataset, the knowledge of the functional relationships present in the cross validation dataset is lost as the datapoints in cross validation dataset are not used for training the ANN model. K fold cross validation is a variant of the cross-validation technique which is especially useful when working with such small datasets and provides a way around this significant limitation [29].

In the K-fold cross validation method, the cross validation procedure is carried out K separate times; each time using a different and mutually exclusive cross validation set chosen randomly from the input data. Thus if there are a total of m training examples in the input dataset, then k different disjoint subsets of equal size *m/k* are randomly selected from the input dataset. Then every time one out of those k disjoint subset is used for cross validation, whereas all the remaining datasets are joined together to form the training dataset. Thus in this method each available datapoint is used for cross validation at least one time and then it is used for training the remaining k-1 times [29].

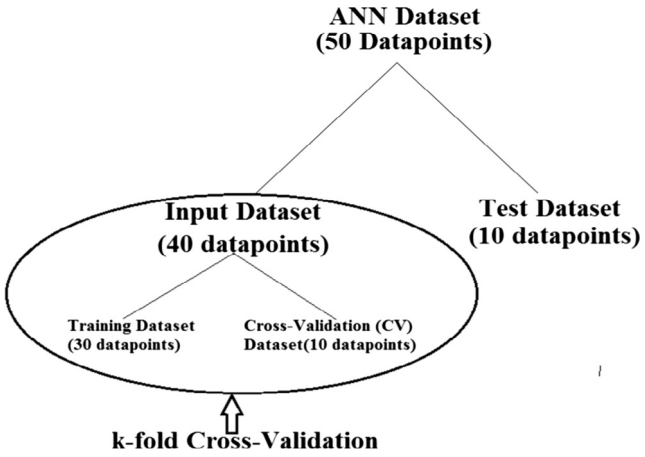

Fig. 3. Complete division of the available ANN dataset consisting of 50 datapoints.

For this research, a 4-fold cross validation was used on the available input dataset of 40 datapoints to generate 4 distinct training and cross validation set combinations, so as to ensure the optimal use of limited available data and for preventing overfitting [41]. Thus for the training of every individual ANN model, there was a training dataset with 30 datapoints and a cross-validation dataset with 10 datapoints available. During the individual ANN model training, the error on training (training error) and cross-validation dataset (CV error) was measured and plotted after every iteration as shown in Fig. 4.

Initially the error fell for both training and cross-validation dataset as learning occurred but after a point the cross-validation error started increasing as the model started to overfit on the data in the training set. Thus the final weights for each ANN model were chosen at the point when the error on the cross-validation dataset was minimum to avoid overfitting for each individual model. The training for each ANN model was done for 100,000 training iterations to find the minima in the cross-validation dataset. From the model experimentation on the available data it was discovered that 100,000 iterations were more than sufficient for the model to find its CV error minima [41].

The learning rate used during the gradient descent in backpropagation algorithm determines the step size of the change while updating the weight values after each iteration. During the implementation of the backpropagation algorithm in this research work, the value for the learning rate α was not kept constant but instead was kept dynamic. The initial value for the learning rate was taken as 0.03. During the ANN training the learning rate was adaptively changed by a factor of 0.9, whenever the value of training error increased during an iteration inside the backpropagation algorithm [41].

The number of neurons in each of the hidden layers of the ANN model can significantly affects its final performance. With a greater number of neurons in the hidden layer, the neural network can simulate more and more complicated functional relationships. On the other hand increasing the number of neurons in the hidden layer also leads to higher computational expense being required for the training of the model. More importantly, increasing the number of neurons leads to an increase in difficulty of finding an optimal error minima during the training of the model [41]. Increasing the number of neurons leads to an increase in the number of weights defining the model and this in turn leads to an increase in the dimensions of the hypothesis space in which we are searching for the error minima. Higher dimensional hypothesis space leads to a highly complicated error surface with many sub-optimal local minimas, which increases the difficulty of finding the optimal error minima during the training of the model. Also because of random initialization of the initial weight connections of neurons in ANN model before its training, it is not possible to empirically determine the optimal number of neurons for each hidden layer [41]. Those initial values of the weights of the neural network determine the starting point in the hypothesis space from which neural network starts it search for finding the error minima during its training. Different random initialization means that each time the neural network starts from a different point in the hypothesis space and follows a different path during its training. It means that after the training, neural networks initialized with different random weights might end up at a different points in the hypothesis space even though they were trained using the same data and had the same network topology. Thus, as the final performance of the ANN model is affected by both network topology and random initialization, it is not possible to isolate the effect of network topology on the final performance. Thus trying different network topologies and comparing their final performance cannot be conclusive as there is no way to know whether the final model

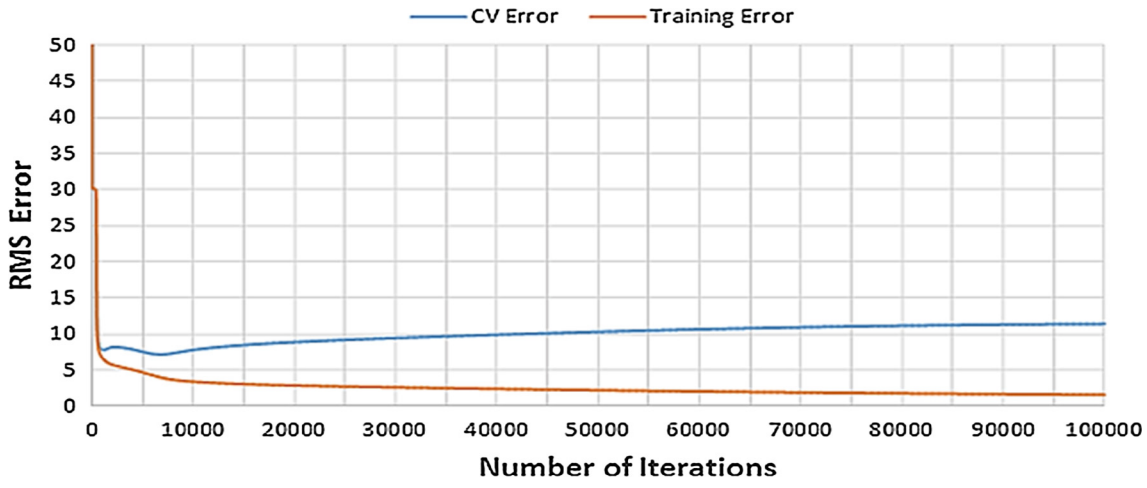

Fig. 4. RMS error for training and cross-validation (CV) datasets versus number of iterations for backpropagation algorithm for a given ANN model.

performance was a result of the particular network topology or the random weight initialization.

Thus the number of neurons in each of the two hidden layer was varied between 10, 15 and 20 and corresponding to two hidden layers that gave rise to a total of 9 ANN models with 9 different network topologies. Each of these nine neural network topologies were trained on all the 4 different combinations of training and cross-validation datasets generated using the 4-fold cross validation technique. Finally for each neural network topology and particular training and cross validation set combination, 5 different random initializations were performed to account for the effect of different starting points in the hypothesis space on the final model performance. In the end a total of 180 different ANN models were developed using the input dataset.

5.2. Development of prediction uncertainty bars

All the 180 models generated were assembled together in order to form the final committee of the models. This committee of the 180 models will be henceforth be referred to as *'the final ANN model'*. Any input data is fed into all the 180 members of the committee and the final output of the committee is the mean of the individual outputs of the members of the committee. The predictions made by the final ANN model are based on the limited knowledge that was present in the input dataset which was used for training and development of the model. Since the input dataset is a sample from the entire population of all possible points in the experimental space, it is not possible for the entire knowledge of the experimental space to be captured by the input dataset [41]. Thus for the predictions made by the final ANN model to be reliable, it is necessary to provide uncertainty bars for those predictions.

Each member of the committee arrives at different error minimas in the hypothesis space corresponding to their network topology, while they are trying to learn the same functional relationships from the limited knowledge present in the given input dataset. Based on the error minimas where they have finished at the end of their training, each member of the committee makes predictions that moderately vary from the predictions made by other members. Thus a measurement of the standard deviation in the predictions made by different members of the final committee is representative of the uncertainty in the prediction which can be made based of the limited knowledge present in the input dataset [41]. The standard deviation in the predicted value of each phase for a given input value by the committee members was measured and then the uncertainty bar for that prediction was calculated using the formula below:

$$\textit{Uncertainty Bar} = \pm 2 \times \textit{Measured standard deviation} \quad (1)$$

The factor of two for measured standard deviation was selected as approximately 95% of observations always fall within two standard deviations from the mean. Hence each individual prediction made by the final ANN model will be of the following form:

$$\textit{Mean Phase Volume Prediction} \pm 2 \times \textit{Standard Deviation} \quad (2)$$

Using this approach for calculating the uncertainty bar allows the final ANN model to generate customized uncertainty bars for each individual phase fraction predictions. There isn't any fixed rigid uncertainty bar for the final model. This approach allows the final model to generate customized uncertainty bars for each prediction based on how confident it is about that prediction. Since the final ANN model is making output predictions based on the knowledge that it has learnt from the input dataset, it will be able to make prediction with greater confidence if the new data is closer to the data which was used for its training in terms of Euclidean distance in the experimental space. But at the same time if the final ANN model faces new data which is far apart, then the uncertainty in its prediction will increase. Using this statistical approach for the uncertainty measurement allows us to capture the localized variations in the confidence of predictions made by the final ANN model [41].

6. Model validation and performance analysis

After the final ANN model had been developed, the model's prediction performance was rigorously analyzed and validated by measuring it against experimental data present in both the input dataset and test dataset.

Initially the models performance on the experimental data in the input dataset was measured. A good analogy for explaining the significance of measuring the ANN model's performance on the input dataset would be the significance of measuring how well a line fits the datapoints in linear regression. Just as a good fit indicates that the predicted line successfully captures the linear nature of the relationship present in the data, so does the model's good performance on the input dataset indicate that it has successfully managed to capture the functional relationships present in the input data. But the performance of the ANN model over the input dataset does not offer any insight about the generalization capabilities of the model when faced with new data. Thus for the final

ANN model validation, the model performance was evaluated by measuring its performance on the completely new and independent experimental data present in the test dataset. The final ANN model had never seen the experimental data in the test dataset before and this validation was akin to testing the predictions made by a theoretical model against independent experimental data. This validation gave an estimate about the robustness and reliability of the final ANN model when faced with completely new data.

For measuring the final ANN model performance on the input dataset, the thermal and mechanical history data of all the Gleeble samples present in the input dataset was fed into the model and the model's predictions were compared with the actual measured phase fraction values obtained from nanoindentation testing. This corresponds to 40 different samples present in input dataset and hence the final ANN model made a total of 120 phase volume fraction predictions. The comparison of all predicted phase volume fraction values against measured values for each ferrite, bainite and martensite phase for input dataset is presented in Fig. 5a, b and c respectively with all the volume fraction values being converted to percentages. Also in Fig. 5, all the measured values have been arranged in the ascending order and all the predictions have been shown along with their calculated uncertainty bars. For the input dataset, the predictions made by the final ANN model are in excellent agreement with the observed experimental phase fraction values. The Root Mean Square (RMS) prediction error measured for the ANN model over the entire input dataset was calculated to be 5.4%. And for 91 out of the 120 phase volume fraction predictions made by the ANN model over the input dataset, the individual prediction error was found to be less than 5.4%.

Now in order to measure the generalization capabilities of the model and its true robustness and reliability, a further validation of the model was done by measuring its performance on completely new independent data in test dataset. The final ANN model

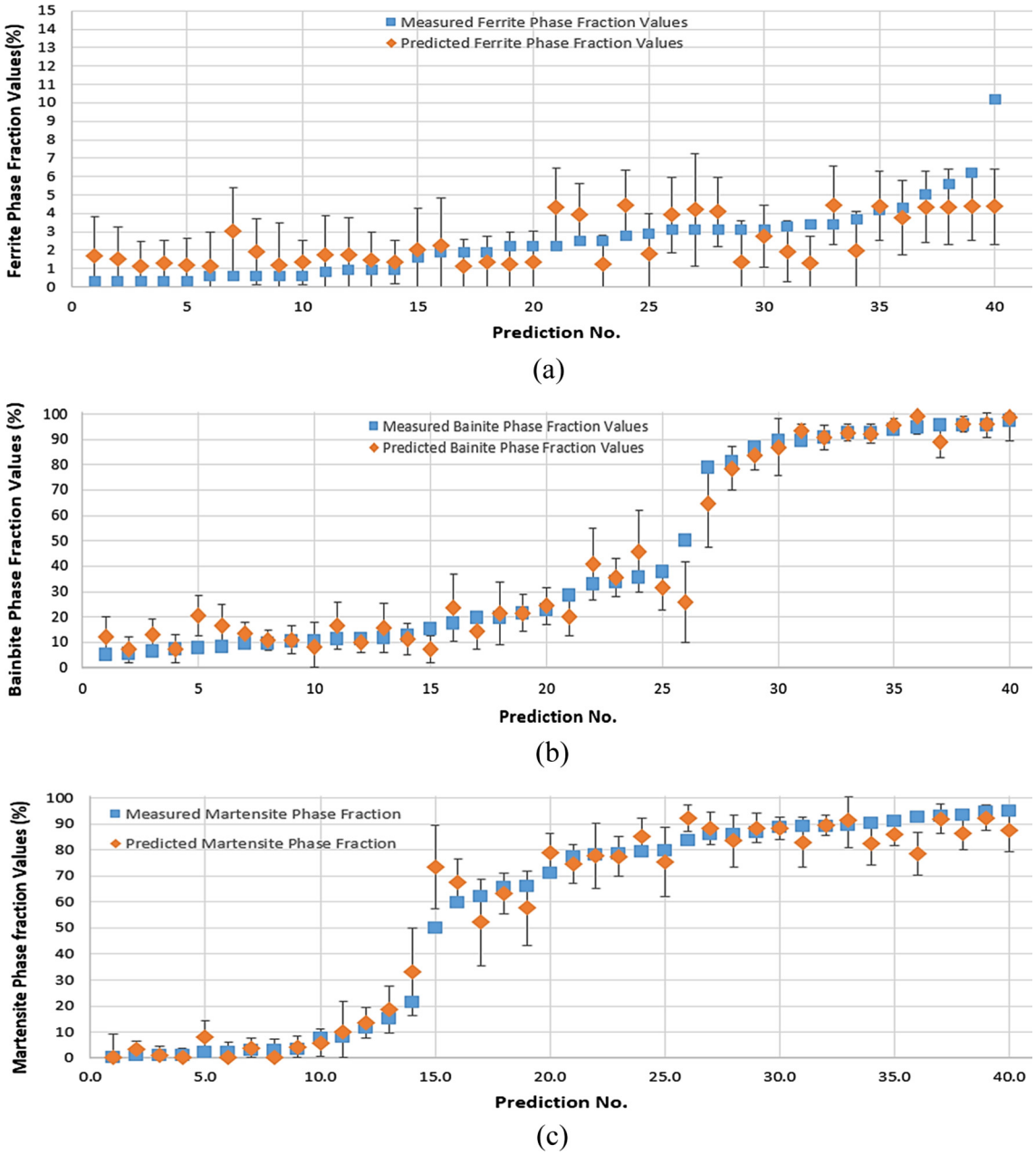

Fig. 5. ANN model phase volume fraction predictions for input dataset (a) Ferrite, (b) Bainite and (c) Martensite (data from 40 Gleeble tests).

has never been exposed to the data in the test dataset before and this was completely unknown data for the model. In order to measure the ANN model's performance on the test dataset, the thermal and mechanical history data from the samples in the test dataset was used as input for the ANN model. Based on that input, the ANN model predicted the final phase distribution in the microstructure for all those Gleeble test samples. This corresponds to 10 different samples present in test dataset and hence the final ANN model made a total of 30 phase volume fraction predictions. The comparison of all predicted values against measured values for each ferrite, bainite and martensite phase for test dataset is presented in Fig. 6a, b and c respectively with all the volume fraction values having been converted to corresponding percentages. Also in Fig. 6, all the measured values have been arranged in the ascending order and all the predictions have been shown along with their calculated uncertainty bars.

The generalization Root Mean Square (RMS) prediction error for the ANN model over the 30 phase volume fraction predictions for the test dataset was calculated to be 7.7%. And for 22 out of the 30 phase volume fraction predictions made by the ANN model over the test dataset, the individual prediction error was found to be less than 7.7%. The RMS performance of the ANN model slightly deteriorated on test set as compared to its performance on the input dataset. This small deterioration in the model performance over test dataset was a result of the model having to make predictions on completely new and unknown data present in the test set.

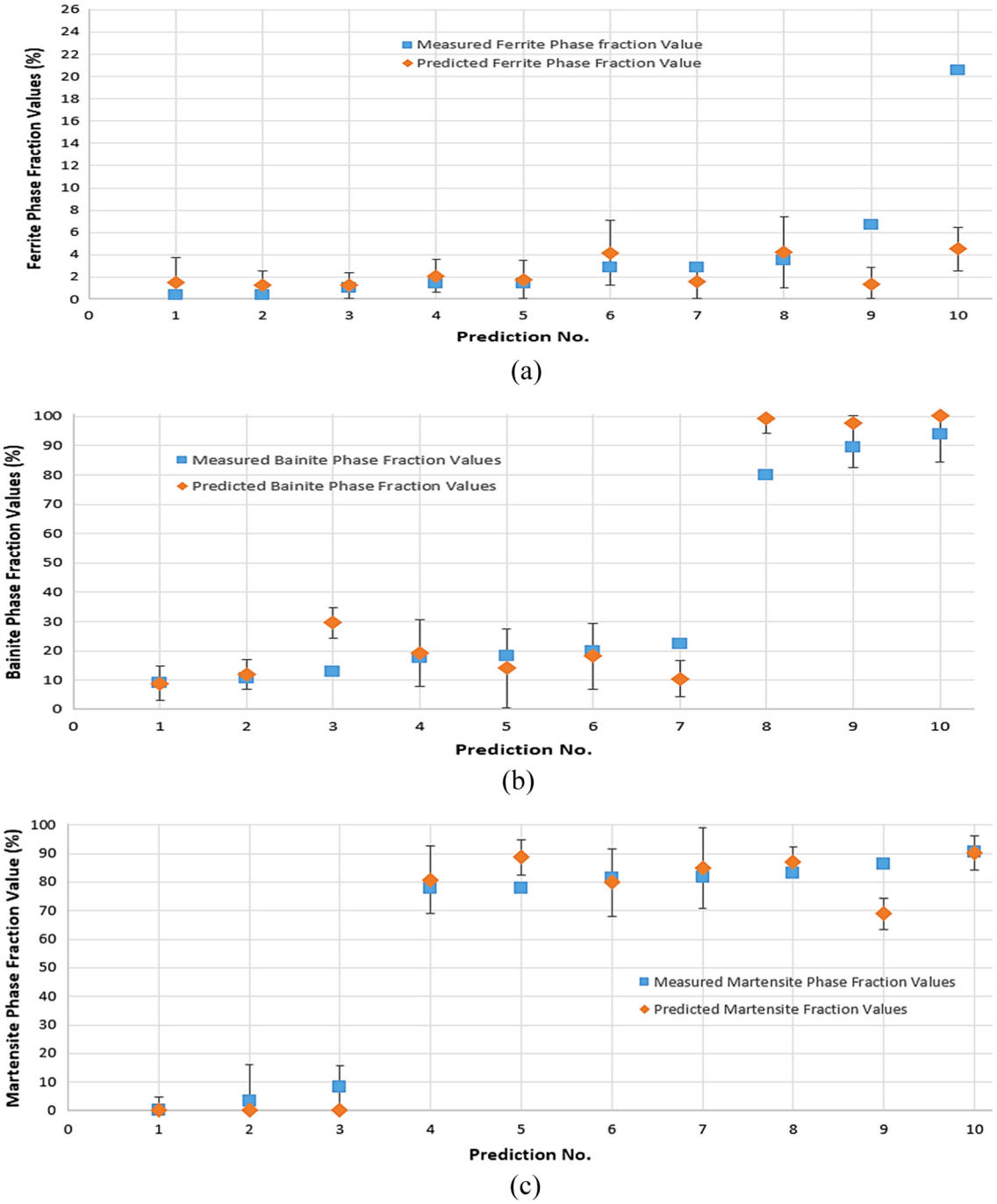

Fig. 6. ANN model phase volume fraction predictions for test dataset (a) Ferrite, (b) Bainite and (c) Martensite (data from 10 Gleeble tests).

Occurrence of this only small amount of actual deterioration in model performance over completely new and independent data offered direct evidence of the robustness and reliability in the predictions made by the final ANN model.

For benchmarking purpose, a standard one hidden and one output layer feedforward neural network was trained using the GUI 'nftool' from Neural Network toolbox in Matlab without using any of the advanced statistical techniques described in this work. In the hidden layer 20 sigmoidal neurons were used, whereas the output layer consisted of 3 linear neurons corresponding to 3 phases. The available 50 datapoints in the ANN dataset were divided randomly into 30 datapoints for training, 10 datapoints for validation and 10 datapoints for test set. The 'trainlm' function in Matlab corresponding to Levenberg-Marquardt backpropagation algorithm with the default values for all parameters was used for training this benchmark model. The generalization RMS prediction error obtained by this benchmark model over the completely new and unknown data in the test set was 12.2%, which is significantly higher than the generalization RMS prediction error of 7.7% obtained by the final ANN model developed in this work over the data in test set. Also the biggest observed absolute difference between the predicted and target phase fraction value was 30% by the benchmark model during its testing.

Now from a total of 30 predictions made by the final ANN model for the test dataset, only 6 predictions differed from the measured values by more than 10% with the biggest observed difference being of 19% (Fig. 6b - Prediction 8). Now for each Gleeble sample in the test set the final ANN model had made three separate phase volume fraction predictions, one each for volume fraction of the ferrite, bainite and martensite phase present in that sample. Thus the 6 predictions which differed from measured values by more than 10% in the test set correspond to 3 different Gleeble samples. The microstructural images corresponding to each of those 3 Gleeble test samples obtained by using metallography and optical microscopy are presented in Fig. 7 along with their predicted and measured phase volume fraction values.

As can be seen, the microstructures in Fig. 7a and b consist mostly of acicular martensitic structure along with small amounts of bainite present in it which support the high martensite phase fraction predictions made by the final ANN model for those samples. The microstructure in Fig. 7c is observed to consist mainly of fine non-lamellar bainite along with a very small fraction of granular ferrite, which also matches the high bainite content predicted by the final ANN model for that sample. Also the measured values for phase fractions obtained by nanoindentation testing have an inherent uncertainty of ~11.7% as calculated based on

Phases	**Measured**	**Predicted**
Martensite	78	89
Bainite	22	10
Ferrite	0	1

(a)

Phases	**Measured**	**Predicted**
Martensite	86	69
Bainite	12	29
Ferrite	1	2

(b)

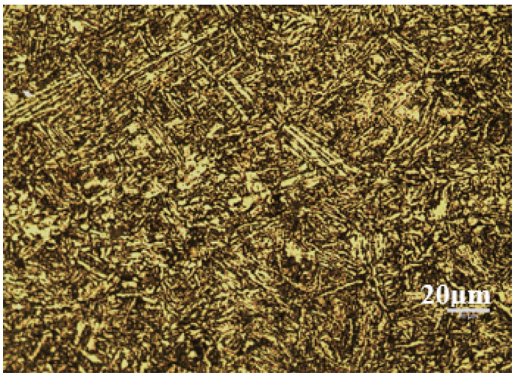

Phases	**Measured**	**Predicted**
Martensite	0	0
Bainite	80	99
Ferrite	21	4

(c)

Fig. 7. Microstructures of Gleeble samples in test set for which the prediction differs from measured phase volume fraction values by more than 10%.

the secondary set of nanoindentation tests (Section 4). When that measurement uncertainty is taken into account, it further supports the predictions made by the final ANN model and establishes the robustness and reliability of the model for making the final phase distribution prediction for tailored hot stamping process.

The experimental data in the test dataset was completely randomly chosen from the original ANN dataset and had thermo-mechanical physical simulation data corresponding to both high die temperatures (highest 823 K) and low die temperatures (Room temperature) for a variety of different deformation temperatures (highest 1133 K and lowest 973 K) and different deformation amounts (highest strain class 50–55% and lowest strain class 0–5%). Thus the final ANN model had been validated against wide range of different thermo-mechanical conditions that occur during tailored hot stamping. This excellent performance of the final ANN model with an RMS error of just 7.7% for phase fraction prediction over the test dataset establishes that the final ANN model has indeed robustly learned the functional relationship between the thermal history, deformation amount and deformation temperature and the final resulting phase distribution in the boron steel. Thermal history, deformation amount and deformation temperature are the factors which have the greatest influence on the final phase distribution during tailored hot stamping and hence were used for development of the current ANN model [8,10,12,15,35,36,48,49]. There are other process parameters such as strain rate, austenitization temperature and austenitization time which also have limited influence on the final phase distribution during tailored hot stamping. All these process parameters can be investigated and added to the final ANN model for gaining further incremental improvements in model's performance.

7. Conclusion

For the first time, an ANN based model was developed for phase distribution prediction during tailored hot stamping. This ANN based model successfully takes into account the thermal history, deformation amount and deformation temperature as inputs for prediction of the final phase distribution for tailored hot stamping. The final developed ANN model gave an excellent performance during its validation over new and independent experimental data and established the robustness and reliability of model's generalization capabilities. This ANN based model used advanced statistical techniques for optimal utilization of the data, for preventing overfitting and for calculating customized uncertainty bars for predictions. Along with that this statistical approach also helped in exploring different neural network topologies and utilizing the unique benefits that each individual topology had to offer for the final ANN based model. The main research findings from this work are as presented below:

1. *Artificial Neural Network (ANN)* based approach was well suited for solving this complex scientific and industrial challenge of final phase distribution prediction in automotive structural and safety components produced by tailored hot stamping process.
2. The developed ANN based model for phase distribution prediction during tailored hot stamping was able to successfully account for the effect of thermal history, deformation amount and deformation temperature on the final microstructures.
3. The Root Mean Square (RMS) error in phase volume fraction prediction performance of the ANN based model was found to be just 5.4% on the input dataset and 7.7% on the test dataset. The reliability and robustness of the ANN model was demonstrated by validating its performance against the completely new and independent experimental data in test set.
4. This prediction performance of the ANN model was a significant improvement over the currently available existing phase distribution prediction models which use only thermal history for making their phase distribution predictions.
5. Different statistical techniques used during the training and development of the final ANN model helped in making it highly robust and reliable. Application of these statistical techniques is highly recommended, especially for the field of empirical modelling in material science, where usually the cost associated with generating experimental data is high and because of that mostly limited experimental data is available for modelling.

Thus the developed final ANN model in this research addresses a critical scientific and industrial challenge faced by the automotive industry and is well suited for *computer aided engineering (CAE)* applications for tailored hot stamping process in the future.

Acknowledgement

The authors would like to thank Tata Steel for providing the material for the research. The authors are deeply grateful for the valuable inputs and support provided by Mr. David Norman, Tata Steel Automotive Engineering group, Mr. Guido Hensen, Tata Steel IJmiuden Technology centre and Dr. Zul Husain, Tata Steel Swinden Technology Centre. Authors are also deeply grateful to Dr. Carl Slater for facilitating the Gleeble testing at University of Birmingham and to Dr. James Bowen and Science City Research Alliance for facilitating the instrumented nanoindentation testing at School of Chemical Engineering, University of Birmingham. Finally authors thankfully acknowledge all the support and assistance provided by the department of WMG, University of Warwick.

References

[1] Karbasian H, Tekkaya AE. A review of hot stamping. J Mater Process Technol 2010;210(15):2103–18.
[2] Zhou J, Wang B, Huang M. Two constitutive descriptions of boron steel 22MnB5 at high temperature. Mater Des 2014;63:738–48.
[3] Lee RS, Lin YK, Chien TW. Experimental and theoretical studies on formability of 22MnB5 at elevated temperatures by Gleeble simulator. Procedia Eng 2014;81:1682–8.
[4] Merklein M, Lechler J. Investigation of the thermo-mechanical properties of hot stamping steels. J Mater Process Technol 2006;177(1–3):452–5.
[5] Abbasi M, Naderi M, Saeed-Akbari A. Isothermal versus non-isothermal hot compression process: a comparative study on phase transformations and structure–property relationships. Mater Des 2013;45:1–5.
[6] Merklein M, Svec T. Hot stamping – manufacturing functional optimized components. Prod Process Prod Eng 2013;7(2):141–51.
[7] Banik J, Lenze FJ, Sikora S, Laurenz R. Tailored properties—a pivotal question for hot forming. In: Proceedings 3rd international conference hot sheet metal forming of high-performance steel—CHS2 (Germany); 2011.
[8] Maikranz-Valentin M, Weidig U, Schoof U, Becker H, Steinhoff K. Components with optimised properties due to advanced thermo-mechanical process strategies in hot sheet metal forming. Steel Res Int 2008;79(2):92.
[9] George R, Bardelcik A, Worswick MJ. Hot forming of boron steels using heated and cooled tooling for tailored properties. J Mater Process Technol 2012;212(11):2386–99.
[10] Svec T, Merklein M. Tailored tempering—heat transfer and resulting properties in dependency of tool temperatures. In: Proceedings 3rd international conference hot sheet metal forming of high-performance steel – CHS2; 2011.
[11] Merklein M, Wieland M, Lechner M, Bruschi S, Ghiotti A. Hot stamping of boron steel sheets with tailored properties – a review. J Mater Process Technol 2016;228:11–24.
[12] Barcellona A, Palmeri D. Effect of plastic hot deformation on the hardness and continuous cooling transformations of 22MnB5 microalloyed boron steel. Metall Mater Trans 2009;40A:1160–74.
[13] Merklein M, Svec T. Transformation kinetics of the hot stamping steel 22MnB5 in dependency of the applied deformation on the austenitic microstructure. In: Hashimoto S, Jansto S, Mohrbacher H, Siciliano F, editors. Proceedings of the IDDRG 2010 international conference. Austria: Graz; 2010.
[14] Min J, Lin J, Min Y, Li F. On the ferrite and bainite transformation in isothermally deformed 22MnB5 steels. Mater Sci Eng A 2012;550:375–87.
[15] Nikravesh M, Naderi M, Akbari GH, Bleck W. Phase transformations in a simulated hot stamping process of the boron bearing steel. Mater Des 2015;84:18–24.

[16] Akerstrom P, Oldenburg M. Austenite decomposition during press hardening of a boron steel – computer simulation and test. J Mater Process Technol 2006;174(1–3):399–406.
[17] Behrens BA, Olle P, Schafer F, Schaffner C. Numerical simulation of microstructural evolution during hot stamping process. In: Proceeding of international deep drawing research group (IDDRG) conference, Hungary; 2007.
[18] Bok HH, Lee MG, Pavlina EJ, Barlat F, Kim HD. Comparative study of the prediction of microstructure and mechanical properties for a hot-stamped B-pillar reinforcing part. Int J Mech Sci 2011;53(9):744–52.
[19] Hochholdinger B, Lorenz D, Erhart T, Schill M. An advanced material model for the prediction of phase fractions and vickers hardness in hot stamping processes. In: Hora P, editor, Proceedings of the IDDRG 2013. ETH Zurich: Institute of Virtual Manufacturing; 2013. p. 279–84.
[20] Tang BT, Bruschi S, Ghiotti A, Bariani PF. Numerical modelling of the tailored tempering process applied to 22MnB5 sheets. Finite Elem Anal Des 2014;81:69–81.
[21] Bhadeshia HKDH. Neural networks in material science. Iron Steel Inst Jpn Int 1999;39(10):966–79.
[22] Tan W, Liu ZY, Wu D, Wang GD. Artificial neural network modeling of microstructure during C-Mn and HSLA plate rolling. J Iron Steel Res Int 2009;16(2):80–3.
[23] Kusiak J, Kuziak R. Modelling of microstructure and mechanical properties of steel using the artificial neural network. J Mater Process Technol 2002;127(1):115–21.
[24] Cetinel H, Ozyigit HA, Ozsoyeller L. Artificial neural networks modeling of mechanical property and microstructure evolution in the Tempcore process. Comput Struct 2002;80(3–4):213–8.
[25] Bhattacharyya T, Singh SB, Sikdar (Dey) S, Bhattacharyya S, Bleck W, Bhattacharjee D. Microstructural prediction through artificial neural network (ANN) for development of transformation induced plasticity (TRIP) aided steel. Mater Sci Eng, A 2013;565:148–57.
[26] Khalaj G, Yoozbashizadeh H, Khodabandeh A, Nazari A. Artificial neural network to predict the effect of heat treatments on Vickers microhardness of low-carbon Nb microalloyed steels. Neural Comput Appl 2013;22(5):879–88.
[27] Guo Z, Sha W. Modelling the correlation between processing parameters and properties of maraging steels using artificial neural network. Comput Mater Sci 2004;29(1):12–28.
[28] Cool T, Bhadeshia HKDH, MacKay DJC. The yield and ultimate tensile strength of steel welds. Mater Sci Eng A 1997;223(1-2):186–200.
[29] Mitchell T. Machine learning. McGraw Hill International Edition; 1997.
[30] Bhadeshia HKDH, Dimitriu RC, Forsik S, Pak JH, Ryu JH. Performance of neural networks in materials science. Mater Sci Technol 2009;25(4):504–10.
[31] Merklein M, Lechler J. Determination of material and process characteristics for hot stamping processes of quenchenable ultra high strength steels with respect to a FE-based process design. SAE Int J Mater Manuf 2009;1(1):411–26.
[32] Geiger M, Merklein M, Hoff C. Basic investigations on the hot stamping steel 22MnB5. Adv Mater Res 2005;6:795–804.
[33] Turetta A, Bruschi S, Ghiotti A. Investigation of 22MnB5 formability in hot stamping operations. J Mater Process Technol 2006;177(1):396–400.
[34] Saeed-Akbari A. Determination of steels microstructural component based on novel characterization techniques [Master thesis]. RWTH Aachen: Institute of Ferrous Metallurgy; 2008.
[35] Naderi M, Saeed-Akbari A, Bleck W. The effects of non-isothermal deformation on martensitic transformation in 22MnB5 steel. Mater Sci Eng, A 2008;487(1–2):445–55.
[36] Nikravesha M, Naderi M, Akbari GH. Influence of hot plastic deformation and cooling rate on martensite and bainite start temperatures in 22MnB5 steel. Mater Sci Eng, A 2012;540(1):24–9.
[37] Naderi M, Saeed-Akbari A, Bleck W. Quantitative and qualitative investigation of the heterogeneous microstructures using surface hardness mapping and dilatation data. Mater Lett 2008;62:1132–5.
[38] Naderi M, Ketabchi M, Abbasi M, Bleck W. Analysis of microstructure and mechanical properties of different high strength carbon steels after hot stamping. J Mater Process Technol 2011;211(6):1117–25.
[39] Honeycombe RWK. Steels-microstructure and properties. 2nd ed. Edward Arnold; 1995.
[40] Cybenko G. Continuous valued neural networks with two hidden layers are sufficient. Center for Supercomputing Research and Development, University of Illinois at Urbana-Champaign; 1988.
[41] Chokshi P. Development of an Artificial Neural Network (ANN) based phase distribution prediction model for 22MnB5 boron steel during tailored hot stamping [Ph.D. thesis]. WMG, University of Warwick; 2016.
[42] Refaeilzadeh P, Tang L, Liu H. Cross-validation. In: Encyclopedia of database systems. Springer US; 2009. p. 532–8.
[43] Sola J, Sevilla J. Importance of input data normalization for the application of neural networks to complex industrial problems. IEEE Trans Nucl Sci 1997;44(3):1464–8.
[44] Geman S, Bienenstock E, Doursat R. Neural networks and the bias/variance dilemma. Neural Comput 1992;4(1):1–58.
[45] Sharkey AJC. On combining artificial neural nets. Connection Sci. 1996;8(3–4):299–314.
[46] Hansen LK, Salamon P. Neural network ensembles. IEEE Trans Pattern Anal Mach Intell 1990;12(10):993–1001.
[47] Arlot S, Celisse A. A survey of cross-validation procedures for model selection. Stat Surv 2010;4:40–79.
[48] Zhou J, Wang B, Huang M, Cui D. Effect of hot stamping parameters on the mechanical properties and microstructure of cold-rolled 22MnB5 steel strips. Int J Miner Metall Mater 2014;21(6):544–55.
[49] Steinbeiss H, So H, Michelitsch T, Hoffmann H. Method for optimizing the cooling design of hot stamping tools. Prod Eng Res Dev 2007;1(2):149–55.